A CMOS-MEMS CC-BEAM METAL RESOSWITCH FOR ZERO QUIESCENT POWER RECEIVER APPLICATIONS

Shi-Chuan Lu, Chun-Pu Tsai, and Wei-Chang Li
Institute of Applied Mechanics, National Taiwan University, Taipei, Taiwan

ABSTRACT

A micromechanical CC-beam resonant switch, a.k.a. resoswitch, based on a 0.35-μm 2-poly-4-metal (2P4M) CMOS-MEMS process platform has been demonstrated. In particular, a 2.1-MHz resoswitch that employs (a) the mode-shape derived displacement difference along its CC-beam structure and (b) generic *VIA* layers available in the CMOS process to achieve displacement gain and metal tungsten-to-tungsten contact yields an average power gain of 23.46 dB when embedded in a simple switched-mode amplifier. Differing from previously reported resoswitches ([1]-[4]), this work demonstrates for the first time resoswitches developed on a standard CMOS process followed by a maskless release step identical to that in [5]. The widely available, low-cost CMOS processes would help expedite the development of resoswitches, which present as enabling components towards zero quiescent power mechanical receivers [2] [3].

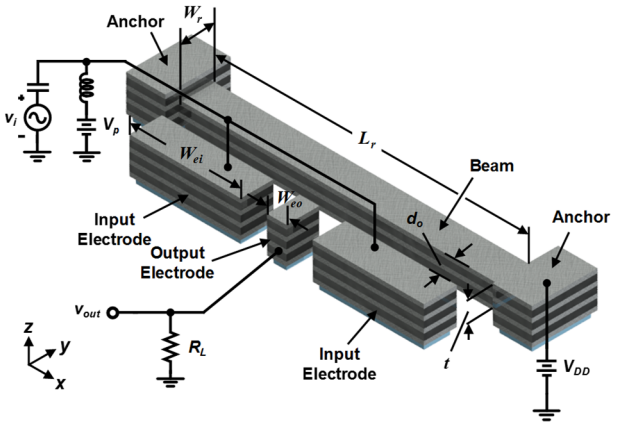

Fig. 1: Schematic of a CMOS-MEMS CC-beam resoswitch, along with the operation scheme.

INTRODUCTION

The recent advances in resoswitches, including AlN folded cantilevers [1], Al displacement amplifying slotted-disk [2], and comb-driven electroplated Au resoswitch for LF receivers [3], all of which have been demonstrated consuming zero quiescent power, have stimulated great interest in employing these devices in sensor RF modules to replace the transistor-based receiver front-ends for extended battery life. Of course, many efforts have also been made to reduce the standby power of transistor-based receivers using innovative architectures and circuit techniques [6] [7]. Nevertheless, it is fundamentally inevitable to operate the front-end transistors with a finite standby current. By utilizing the zero-quiescent power resoswitch, it could become possible to drastically reduce the standby power consumption of the RF module, which, in fact, the most critical portion among the entire sensor components in determining the sensor battery life.

These successfully demonstrated resoswitches of [1]-[4] are all based on low-temperature CMOS-compatible fabrication processes that allow monolithically integration with baseband circuits. However, the processes carried out in the university cleanroom environment involve complicated steps or special tweaks [4] that posts a barrier for wider recognition as it would require numerous evolution cycles, that is, lots of money, towards mass production.

On the other hand, standard CMOS processes have been proven as fabrication platforms for vibrating MEMS devices [5] [8] [9]. In contrast to university cleanroom processes, foundry based CMOS-MEMS process platforms share most of the advantages of mature CMOS technology—low cost, fast prototyping, and a high degree of fidelity on process variation and device performance.

This work exploits a standard CMOS derived process flow used in [5] for manufacturing MEMS resonators to achieve a metal CC-beam resoswitch for zero quiescent power receiver applications. In particular, the resoswitch deploys the location-dependent displacement along the beam to realize displacement gain—the output has a large displacement magnitude than the input—needed for preventing the input electrodes from impacting, which would otherwise corrupt the driving signal and even cause electrical shorting failure as the dc bias voltage is being applied on the input electrodes. In addition, the fabrication process results extruded *VIA* layers that form hard refractory metal W contact, which is preferred for enhanced resistance to heat and microwelding [10]. Under a dc bias of 67 V and a driving voltage of 2.09 V_{amp}, the CC-beam resoswitch reaches the switching threshold and yields an average power gain of 23.46 dB at 2.1 MHz when embedded in a simple switched-mode amplifier.

DEVICE STRUCTURE AND OPERATION

Fig. 1 plots the schematic of the CC-beam resoswitch. To operate, the input electrodes are biased with a dc bias V_P and an ac control/driving signal v_i via a bias-T circuit, and a supply voltage V_{DD} is applied on the beam structure. This set-up generates a modulated electrostatic force at the frequency of the driving signal v_i. When the driving frequency matches the resonance frequency of the CC-beam, the CC-beam starts to vibrate transversely—in this case, laterally along the *y*-axis of Fig. 1. The mechanical resonance frequency takes the form

$$f_{nom} = 1.0279\sqrt{\frac{E_{eff}}{\rho_{eff}}}\frac{W_r}{L_r^2} \quad (1)$$

where

$$E_{eff} = \frac{\sum E_i I_i}{\sum I_i} \text{ and } \rho_{eff} = \frac{\sum \rho_i A_i}{\sum A_i} \quad (2)$$

where E_i, I_i, ρ_i and A_i are the Young's modulus, second

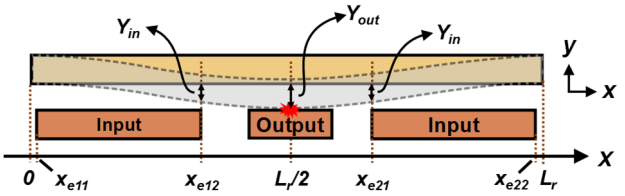

Fig. 2: Schematic of a resoswitch that shows the electrode coordinates and the input and output displacements.

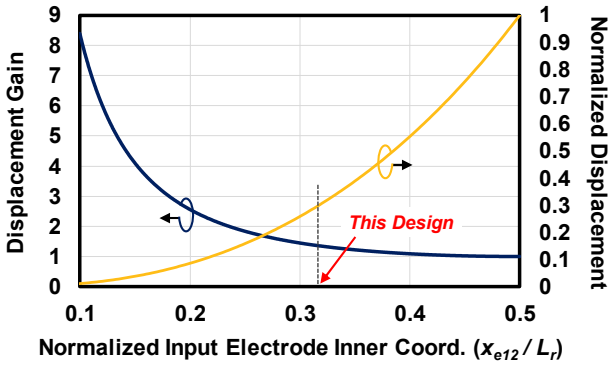

Fig. 3: Displacement gain and normalized output displacement as a function of the coordinate of the inner edge of the input electrode (normalized to the beam length).

moment of area, density, and cross-section area of each structural material. Given that the structural layers include the CMOS layers of *METAL1* through *METAL3*, the effective Young's modulus E_{eff} and ρ_{eff} of the structural composite equal 170.3 GPa and 4632 kg/m^3, respectively.

While the edges of the *VIA* layers are drawn to be flush with the *METAL* layers, the oxide opening is actually overetched, resulting in the *VIA* layers wider than the drawing and therefore extruded W along the structure sidewall. This virtually non-ideal overetching effects a preferred hard refractory metal W-to-W contact that has been discovered exhibiting better resistance to microwelding and wear compared to soft metal, e.g., Al [10].

Displacement Gain vs. Displacement Magnitude

As discussed in [2] and [4], resoswitch devices require displacement amplification to prevent input impacting. Here, the CC-beam resoswitch achieves displacement gain by directly deriving the transverse vibration mode shape. As shown in Fig. 2, via retrieving the input electrodes from the center of the beam, one can achieve an effective displacement gain defined as the displacement magnitude at the center of the beam versus the maximum displacement along the input electrodes. Assuming the two input electrodes are symmetrical to the center of the beam, the coordinates of the inner edges of the input electrodes (*cf.* Fig. 2) determine the displacement gain, taking the form

$$G_{disp} = \frac{Y(L_r/2)}{Y(x_{e12})} = \frac{Y(L_r/2)}{Y(x_{e21})} \qquad (3)$$

The CC-beam resoswitch achieves displacement gain at the expense of driving force. The higher the displacement gain, the smaller the input electrode and therefore the driving force. Fig. 3 plots the displacement gain, together with the normalized output displacement

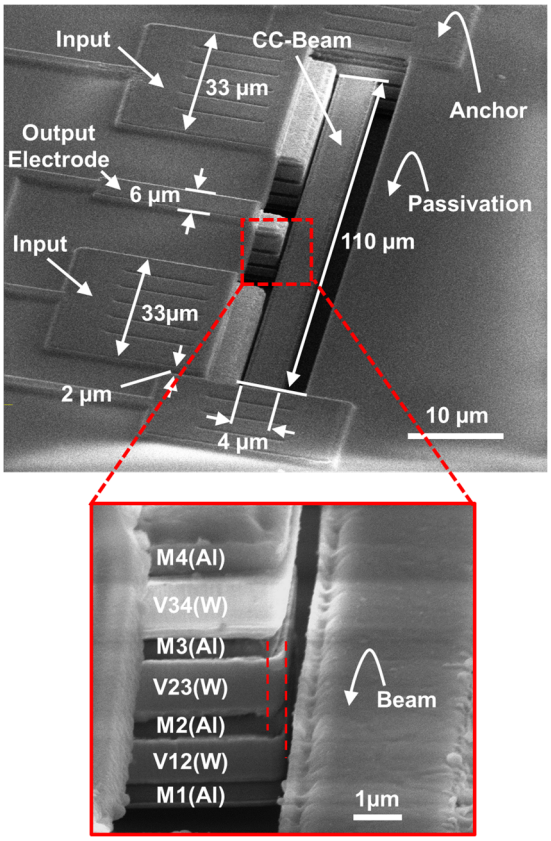

Fig. 4: SEM of a fabricated CMOS-MEMS CC-beam resoswitch and a close-up of the output electrode, showing the metal Al and extruded W layers.

magnitude, to the left and right *y*-axes, respectively, versus the normalized coordinate (to the beam length) of the input electrode inner edge. As discussed, the CC-beam resoswitch trades the overall displacement magnitude for the displacement gain. Here, the designed normalized coordinate x_{e12}/L_r of 0.31 gives a displacement gain of 1.35.

EXPERIMENTAL RESULTS

The fabrication process follows that in [5]. The release step of the standard CMOS fabricated chip utilizes a commercially available Al-compatible HF (Silox Vapox III, Transene Company, Inc.). Fig. 4 presents the SEM photos of a released CC-beam resoswitch, including a zoom-in to the output electrode revealing the structural layers. Note that the CC-beam structure is composed of layers from *METAL1* to *METAL3* while the electrodes are through the entire stack from *METAL1* to *METAL4*. As shown in Fig. 4, the *VIA* layers of metal W extrude for about 100-200 nm along the sidewall.

Frequency Responses

Fig. 5 presents the frequency responses for varying input driving amplitudes, showing the device responses from the linear into the nonlinear regions where the bandwidth widens as the input voltage increases. The resoswitch exhibits an extracted *Q* of 762 when operating in the linear region, i.e., as a regular resonator.

Fig. 6 plots the frequency responses of the resoswitch when the driving signal reaches the switching threshold, where the resoswitch performs a channel-selection type

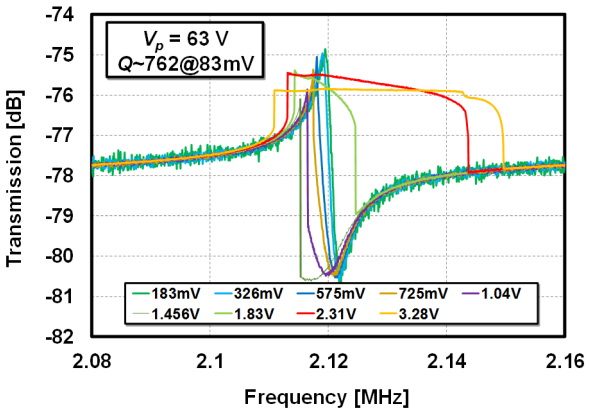

Fig. 5: Measured frequency responses versus varying input signal levels.

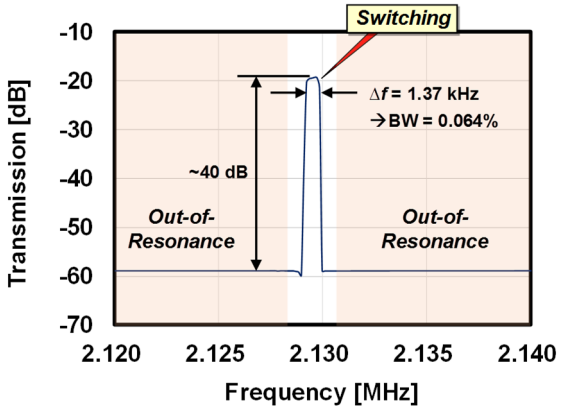

Fig. 6: Measured channel-selection-like filter frequency responses of the resoswitch.

filter response with a sharp roll-off. Note that the device indeed delivers power gain. The measured passband is less than 0 dB because the power delivered by the network analyzer is based upon 50 Ω. The actual input impedance of 1.53 MΩ is much higher than 50 Ω and therefore, the actual delivered input power to the device is substantially lower—by 44.86 dB (i.e., $10\log(1.53\times10^6/50)$)—than that shown on the network analyzer. Thus, the resoswitch-based filter also functions as a power amplifier with a power gain around 25 dB in the passband, which matches with that calculated from the time domain waveforms.

Switching Waveforms

Fig. 7 illustrates the measurement set-up for capturing the switching waveform, in which the CC-beam resoswitch is wire bonded to a PCB with an embedded buffer used to drive the coaxial cable connected to an oscilloscope. The testing board is placed in a custom-built vacuum chamber that allows pressure pumped to below 10^{-5} Torr with a turbo pump.

Fig. 8 shows the switching waveform when the resoswitch input is biased via a bias-T circuit with a dc voltage of 67 V and an ac signal of 2.085 V_{amp}. A dc voltage V_{DD} of 5 V is applied on the CC-beam itself. A discharge resistor of 470 Ω attaches to the resoswitch output. Integrating the signal over the switching period yields an average power gain of 23.46 dB.

As shown in Fig. 8, while the input is driven by a continuous sinusoidal signal, the output switching

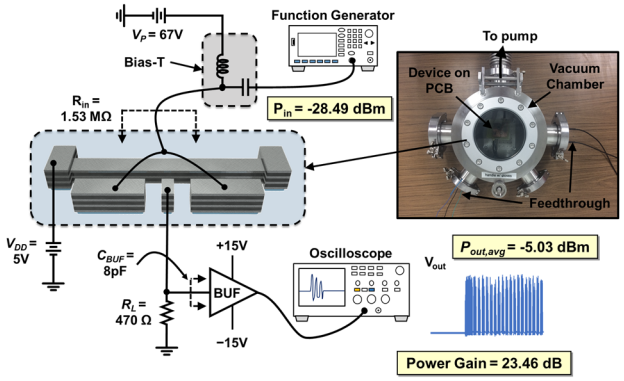

Fig. 7: Schematic of the measurement set-up used to capture the switching output of a resoswitch-embedded switched-mode amplifier.

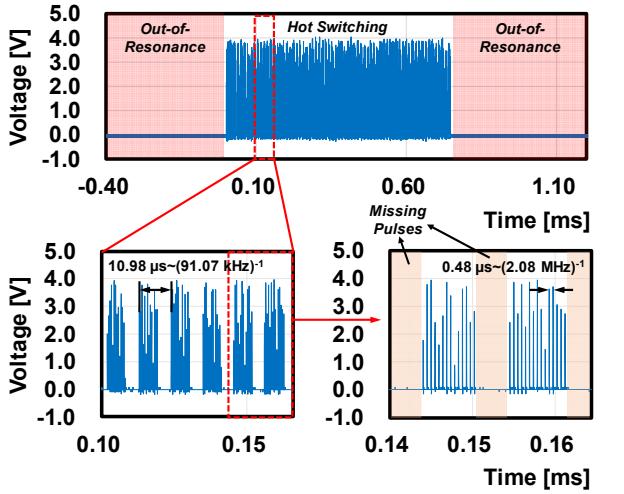

Fig. 8: Captured switching waveform using the set-up of Fig. 7, where the switching pulses seem to be gated by a frequency around 91 kHz caused by the squegging effect.

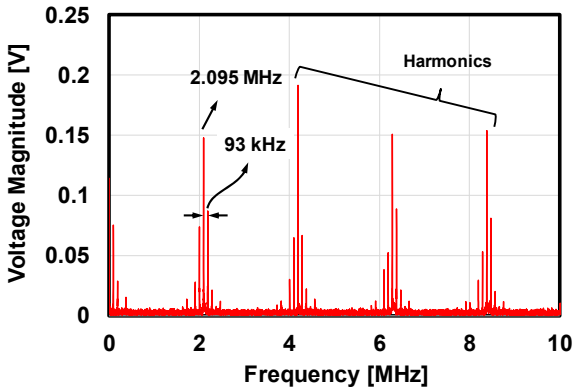

Fig. 9: Frequency domain of the switching waveform of Fig. 8, illustrating the fundamental tone at the resonance frequency of 2.1 MHz and its harmonics mixed with a 93-kHz modulation signal.

waveform exhibits amplitude modulated envelopes at a modulating frequency around 91 kHz. Applying FFT to the switching data confirms the observation that the frequency domain of the waveform contains the strong fundamental tone of the resonance frequency mixed with a signal at a lower frequency around 93 kHz (*cf.* Fig. 9). The low-frequency modulation that yields periodic disappearing

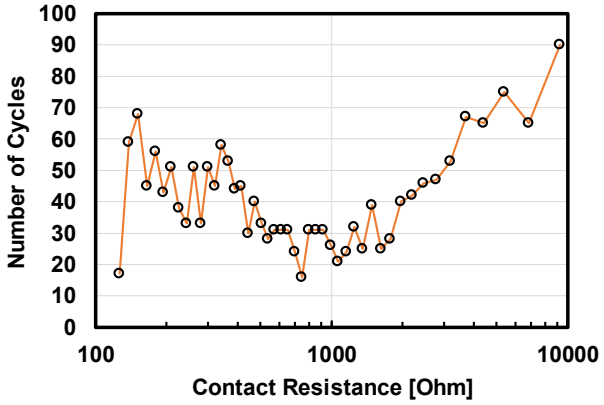

Fig. 10: Number of switching cycles as a function of contact resistance back calculated from the switching waveform of Fig. 8.

pulses (very likely) results from the squegging effect discovered in a previous work of [11]. Further investigation is required to fully understand the phenomenon, for example, how the squegging frequency relates to the contact properties and ways to mitigate the squegging issue.

Note that the switching waveform of Fig. 8 exhibits varying pulse magnitudes, indicating that the dynamic contact resistance is unstable. Fig. 10 plots the number of cycles versus the back-calculated contact resistance for the captured switching signal of Fig. 8. The contact resistance ranges from 126 Ω, much smaller than the static W-to-W contact resistance of ~1 kΩ reported in [10], up to 9.3 kΩ, giving an overall average of 1.8 kΩ. The reduction of contact resistance in the resoswitch results from the strong impulsive contact force generated by impact. Since the number of switching captured in Fig. 8 is nearly 2000 cycles, the increased contact resistance due to the degrading interface after 10^7 cycles shown in [10] is not observed here. While the fluctuant contact resistance could cause issues in resoswitch-based AM receivers [12], resoswitches still could serve well for applications such as wake-up radio front-ends or FM systems that do not transmit information upon the signal amplitude.

CONCLUSIONS

A CMOS-MEMS-based CC-beam resoswitch has been successfully demonstrated that yields an average power gain of 23.46 dB when embedded in a switched-mode amplifier, verifying the capability of CMOS-MEMS process platform used for resoswitch applications. While this work uses the 0.35-µm process as a prototyping vehicle, the true benefit of the CMOS-MEMS platform can be revealed when employing more advanced nodes that allows smaller gap spacing, which in turn would help reduce the input sensitivity. Additionally, although might not being an immediate issue for some applications, the squegging phenomena that induce fluctuation in the output voltage need to be mitigated for reliable and predictable resoswitches. Work towards this goal continues.

ACKNOWLEDGEMENTS

This research was funded by the Ministry of Science and Technology, Taiwan (MOST-103-2221-E-007-113-MY3). The chip fabrication was supported by the Chip Implementation Center (CIC) and Taiwan Semiconductor Manufacturing Company (TSMC), Hsinchu, Taiwan. The authors would like to thank Dr. Ming-Huang Li for valuable discussions and inputs on CMOS-MEMS fabrication process.

REFERENCES

[1] T. Wu, G. Chen, Z. Qian, W. Zhu, M. Rinaldi and N. McGruer, "A Microelectromechanical AlN …," in *Tech. Dig. the 19th Int. Conf. on Solid-State Sensors, Actuators, & Microsystems (TRANSDUCERS'17)*, Kaohsiung, Taiwan, June 18-22, 2017, pp. 2123-2126.

[2] W.-C. Li, Y. Lin and C. T.-C. Nguyen, "Metal Micromechanical Filter-Power Amplifier Utilizing …," in *Tech. Dig. the 17th Int. Conf. on Solid-State Sensors, Actuators, & Microsystems (Transducers'13)*, Barcelona, Spain, June 16-20, 2013, pp. 1445-1448.

[3] R. Liu, J. N. Nilchi, Y. Lin, T. L. Naing and C. T.-C. Nguyen, "Zero Quiescent Power VLF Mechanical …," in *Tech. Dig. the 18th Int. Conf. on Solid-State Sensors, Actuators, & Microsystems (Transducers'15)*, Anchorage, AK, 21-25 June, 2015, pp. 51-54.

[4] Y. Lin, T. Riekkinen, W.-C. Li, E. Alon and C. T.-C. Nguyen, "A Metal µmechanical…," in *Tech. Digest 2012 IEEE Int. Electron Devices Mtg. (IEDM'11)*, Washington, DC, Dec. 5-7, 2011, pp. 162-165.

[5] W.-C. Chen, W. Fang and S.-S. Li, "A generalized CMOS-MEMS platform...," *J. Micromech. Microeng.*, vol. 21, no. 6, June 2011.

[6] J. Ayers, K. Mayaram and T. S. Fiez, "An Ultralow-Power Receiver for Wireless…," *IEEE Journal of Solid-State Circuits,* vol. 45, no. 9, pp. 1759-1769, Sept. 2010.

[7] J. L. Bohorquez, A. P. Chandrakasan and J. L. Dawson, "A 350 µW CMOS MSK Transmitter and 400 µW OOK Super-Regenerative…," *IEEE Journal of Solid-State Circuits,* vol. 44, no. 4, pp. 1248-1259, Apr., 2009.

[8] C.-Y. Chen, M.-H. Li, C.-S. Li and S.-S. Li, "Design and characterization of mechanically…," *Sensors and Actuators A: Physical,* vol. 216, pp. 394-404, 2014.

[9] M.-H. Li, C.-Y. Chen, C.-Y. Liu and S.-S. Li, "A Sub-150µW BEOL-Embedded…," *IEEE Electron Device Letters,* vol. 37, no. 5, pp. 648-651, May 2016.

[10] Y. Chen, R. Nathanael, J. Jeon, J. Yaung, L. Hutin and T.-J. K. Liu, "Characterization of Contact Resistance Stability…," *Journal of Microelectromechanical Systems,* vol. 21, no. 3, pp. 511 - 513, Feb., 2012.

[11] Y. Lin, R. Liu, W.-C. Li and C. T.-C. Nguyen, "Polycide contact…," in *IEEE 27th International Conference on Micro Electro Mechanical Systems (MEMS'14)*, San Francisco, CA, Jan. 26-30, 2014, pp. 1273-1276.

[12] R. Liu, J. N. Nilchi, W.-C. Li and C. T.-C. Nguyen, "Soft-impacting micromechanical resoswitch…," in *IEEE 29th International Conference on Micro Electro Mechanical Systems (MEMS'16)*, Shanghai, China, Jan. 24-28, 2016, pp. 51-54.

CONTACT

*W.-C. Li, Tel: +886-2-33665636; wcli@iam.ntu.edu.tw